Ultra-Wide Bandwidth Time-Hopping Spread-Spectrum Impulse Radio for Wireless Multiple-Access Communications

Moe Z. Win, *Senior Member, IEEE,* and Robert A. Scholtz, *Fellow, IEEE*

***Abstract*—Attractive features of time-hopping spread-spectrum multiple-access systems employing impulse signal technology are outlined, and emerging design issues are described. Performance of such communications systems in terms of achievable transmission rate and multiple-access capability are estimated for both analog and digital data modulation formats under ideal multiple-access channel conditions.**

***Index Terms*—Impulse radio, ultra-wide bandwidth.**

I. Introduction to Impulse Radio Systems

THE TERM *wideband*, as applied to communication systems, can have different meanings. In conventional systems, "wideband" implies a large modulation bandwidth and thus a high data transmission rate. In this paper, a spread-spectrum (SS) system [1]–[4] is described in which the transmitted signal occupies an extremely large bandwidth even in the absence of data modulation. In this case, a signal is transmitted with a bandwidth much larger than the data modulation bandwidth and thus with a reduced power spectral density. This approach has the potential to produce a signal that is more covert, has higher immunity to interference effects, and has improved time-of-arrival resolution.

The SS radio system described here is unique in another regard: it does not use a sinusoidal carrier to raise the signal to a frequency band in which signals propagate well, but instead communicates with a time-hopping (TH) baseband signal composed of subnanosecond pulses (referred to as *monocycles*). Since the bandwidth ranges from near dc to several gigahertz, this *impulse radio* signal undergoes distortions in the propagation process even in benign propagation environments. On the other hand, the fact that an impulse radio system operates in the lowest possible frequency band that supports its wide transmission bandwidth means that this radio has the best chance of penetrating materials that tend to be more opaque at higher frequencies. Finally, it should be noted that the use of signals with gigahertz bandwidths means that multipath is resolvable down to path differential delays on the order of a nanosecond or less, i.e., down to path length differentials on the order of a foot or less. This significantly reduces fading effects even in indoor environments [5], [6].

The capability to highly resolve multipath combined with the ability to penetrate through materials makes impulse technology viable for high-quality, fully mobile short-range indoor radio systems. Lack of significant multipath fading may considerably reduce fading margins in link budgets and allow low transmission-power operation. Low transmission-power and short-range operation with ultra-wide bandwidth (UWB) results in an extremely low transmitted power spectral density, which insures that impulse radios do not interfere with narrow-band radio systems operating in dedicated bands.

Modulation of TH-SS impulse radio is accomplished through the time shifting of pulses. Antipodal modulation cannot be achieved by this means because pulse inversion is not an option in this signaling format. Comparison with direct-sequence code-division multiple-access (DS-CDMA) systems over comparable bandwidths indicates that comparable numbers of users could also be supported by DS-CDMA signals although the spectral shapes of these systems are quite different. However, the authors are not aware of any DS-CDMA systems that operate with gigahertz bandwidths. On the other hand, impulse radios with gigahertz bandwidths have been implemented and demonstrated in single-user links with data rates up to 150 kb/s, and hence the basic principles of operation have been validated.

The key motivations for using TH-SS impulse radio are the ability to highly resolve multipath and the availability of the technology to implement and generate UWB signals with relatively low complexity. The techniques for generating UWB signals have existed for more than three decades [7]. Perhaps it is more readily known to the radar community under its time-domain description as "baseband carrierless short pulse" techniques. A comprehensive reference of early work in this area can be found in [8].

This paper describes a modulation format that can be supported by current technology and presents receiver processing and performance prediction for both analog and digital data modulation formats under ideal multiple-access channel conditions. Real indoor channel measurements and their implications

Paper approved by E. S. Sousa, the Editor for CDMA Systems of the IEEE Communications Society. Manuscript received January 27, 1997; revised May 19, 1998. This work was supported in part by the Joint Services Electronics Program under Contract F49620-94-0022, and in part by the Integrated Media Systems Center, a National Science Foundation Engineering Research Center with additional support from the Annenberg Center for Communication at the University of Southern California and the California Trade and Commerce Agency. The paper was presented in part at the IEEE Fourth International Symposium on Spread-Spectrum Techniques and Applications, Mainz, Germany, September, 1996, and in part at the IEEE International Conference on Communications, Montréal, Canada, June 1997.

M. Z. Win is with the Wireless Systems Research Department, Newman Springs Laboratory, AT&T Laboratories–Research, Red Bank, NJ 07701-7033 USA (e-mail: win@research.att.com).

R. A. Scholtz is with the Communication Sciences Institute, Department of Electrical Engineering-Systems, University of Southern California, Los Angeles, CA 90089-2565 USA (e-mail: scholtz@usc.edu).

Publisher Item Identifier S 0090-6778(00)03632-1.

on signal design and Rake receiver design can be found in [5], [6], [9]–[12].

II. Time-Hopping Format Using Impulses

A typical TH format of the kth impulse radio transmitter output signal $s_{\rm tr}^{(k)}(u,t^{(k)})$ is given by

$$s_{\rm tr}^{(k)}\left(u,t^{(k)}\right)=\sum_{j=-\infty}^{\infty} w_{\rm tr}\left(t^{(k)}-jT_{\rm f}-c_j^{(k)}(u)T_{\rm c}-d_j^{(k)}(u)\right) \tag{1}$$

where $t^{(k)}$ is the transmitter clock time, $w_{\rm tr}(t)$ represents the transmitted monocycle waveform that nominally begins at time zero on the transmitter clock, and the quantities associated with (k) are transmitter dependent.[1] Hence, the signal emitted by the kth transmitter consists of a large number of monocycle waveforms shifted to different times, the jth monocycle nominally starting at time $jT_{\rm f}+c_j^{(k)}(u)T_{\rm c}+d_j^{(k)}(u)$. The structure of each time shift component is described as follows.

1) *Uniform Pulse Train Spacing:* A pulse train of the form $\sum_{j=-\infty}^{\infty} w_{\rm tr}(t^{(k)}-jT_{\rm f})$ consists of monocycle pulses spaced $T_{\rm f}$ seconds apart in time. The *frame time* or *pulse repetition time* typically may be a hundred to a thousand times the monocycle width, resulting in a signal with a very low duty cycle. Multiple-access signals composed of uniformly spaced pulses are vulnerable to occasional *catastrophic collisions* in which a large number of pulses from two signals are received simultaneously, much as might occur in spread ALOHA systems [13].
2) *Random/Pseudorandom TH:* To eliminate catastrophic collisions in multiple accessing, each link (indexed by k) uses a distinct pulse-shift pattern $\{c_j^{(k)}(u)\}$ called *a TH sequence*. These hopping sequences $\{c_j^{(k)}(u)\}$ are pseudorandom with period $N_{\rm p}$, with each element an integer in the range $0 \le c_j^{(k)}(u) < N_{\rm h}$. The TH sequence therefore provides an additional time shift to each pulse in the pulse train, with the jth monocycle undergoing an added shift of $c_j^{(k)}(u)T_{\rm c}$ seconds, which are discrete values between 0 and $N_{\rm h}T_{\rm c}$ seconds. Since the pseudorandom TH sequence has period $N_{\rm p}$, the waveform $\sum_{j=-\infty}^{\infty} w_{\rm tr}(t^{(k)}-jT_{\rm f}-c_j^{(k)}(u)T_{\rm c})$ has period $T_{\rm p}=N_{\rm p}T_{\rm f}$ and has a power spectral density with line spacing $1/T_{\rm p}$.

   It is assumed that $N_{\rm h}T_{\rm c} \le T_{\rm f}$, and hence the ratio $N_{\rm h}T_{\rm c}/T_{\rm f}$ indicates the fraction of the frame time $T_{\rm f}$ over which TH is allowed. Since a short time interval may be required to read the output of a monocycle correlator and to reset the correlator, $N_{\rm h}T_{\rm c}/T_{\rm f}$ may be strictly less than one. If $N_{\rm h}T_{\rm c}/T_{\rm f}$ is too small, then catastrophic collisions remain a significant possibility. Conversely, with a large enough value of $N_{\rm h}T_{\rm c}/T_{\rm f}$ and well-designed TH sequences, the multiple-access interference in many situations can be modeled as a Gaussian random process [14].

[1]In this notation, u represents a point in the underlying probability sample space, and hence random variables are distinguished in this notation by the fact that they are functions of u. If a function does not depend on u, then it is not random. A random process $r(u,t)$ is a different function of t for each u and is a random variable for each value of t.

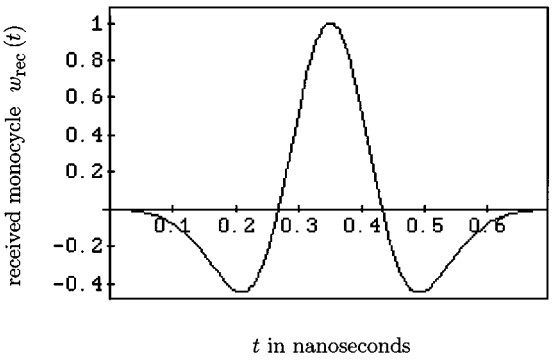

Fig. 1. A typical idealized received monocycle $w_{\rm rec}(t)$ at the output of the antenna subsystem as a function of time in nanoseconds. The model used in this plot is $w_{\rm rec}(t+0.35)=[1-4\pi(t/\tau_m)^2]\exp[-2\pi(t/\tau_m)^2]$ with $\tau_m=0.2877$.

3) *Modulation Schemes:* The sequence $\{d_j^{(k)}(u)\}_{j=-\infty}^{\infty}$ is a sample sequence from a wide-sense stationary random process $d^{(k)}(u,t)$, with samples taken at a rate of $T_{\rm f}^{-1}$. Both analog and digital modulation formats are described in this paper. For the analog impulse radio, analog subcarrier signaling is considered, where stabilization of the tracking S-curve of the clock control loops can be accomplished with a relatively simple receiver design. This signaling format is of particular interest for low power or miniaturized applications. For the digital impulse radio, a pulse position data modulation is considered. For simplicity, it is assumed that the data stream is balanced so that the clock-tracking loop S-curve can maintain a stable tracking point. With more complicated modulation schemes, pulse-shift balance can be achieved in each symbol time.

When $N_{\rm u}$ transmitters are active in the multiple-access system, the composite received signal $r(u,t)$ at the output of this receiver antenna is modeled as

$$r(u,t)=\sum_{k=1}^{N_{\rm u}} A_k s_{\rm rec}^{(k)}(u,t-\tau_k(u))+n(u,t) \tag{2}$$

in which A_k models the attenuation over the propagation path of the signal $s_{\rm rec}^{(k)}(u,t-\tau_k(u))$ received from the kth transmitter. The random variable $\tau_k(u)$ represents the time asynchronism between the clock of the signal received from transmitter k and the receiver clock, and $n(u,t)$ represents other non-monocycle interference (e.g., receiver noise) present at the correlator input.

Even an ideal channel and antenna system modifies the shape of the transmitted monocycle $w_{\rm tr}(t)$ to $w_{\rm rec}(t)$ at the output of the receiver antenna. A typical idealized model of the received pulse shape $w_{\rm rec}(t)$ is shown in Fig. 1. For purposes of analysis, we assume that the true transformed pulse shape $w_{\rm rec}(t)$ is known to the receiver and can be used to determine matched-filter receiving structures.

III. Analog Impulse Radio Multiple-Access Receiver (AIRMA)

A. Impulse Correlator Output Model

A simplified model describing a portion of the AIRMA receiver is shown in Fig. 2. We assume that the receiver is perfectly

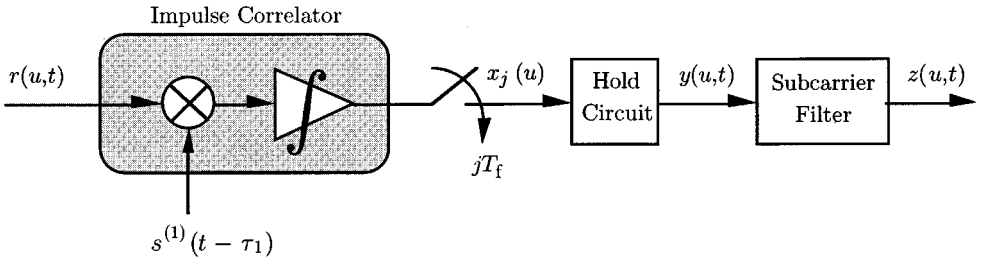

Fig. 2. Simplified model of the analog impulse radio multiple-access receiver front end.

locked to the signal from the first transmitter. That is, the receiver has a replica of the first transmitter's TH sequence $\{c_j^{(1)}\}$ running synchronously with the time hops received via the airwaves from the first transmitter. The implication is that $\{c_j^{(1)}\}$ and τ_1 are no longer random variables from the viewpoint of the receiver. Hence, the signal on the local reference arm of the receiver correlator, coming from the template generator, is simply

$$s^{(1)}(u, t-\tau_1) = \sum_{j=-\infty}^{\infty} w_{\rm cor}\left(t - jT_{\rm f} - c_j^{(1)}T_{\rm c} - \tau_1\right) \quad (3)$$

which looks formally like the received waveform from transmitter 1 with no data modulation imposed on it, but with a different pulse shape $w_{\rm cor}(t)$ in place of the monocycle.

The impulse correlator output is sampled to obtain the sequence $\{x_j(u)\}$ and is held by the sample-and-hold (S/H) device at a rate of one sample per frame. The correlator output corresponding to the jth frame is

$$x_j(u) = \int_{-\infty}^{\infty} r(u,t) w_{\rm cor}\left(t - jT_{\rm f} - c_j^{(1)}T_{\rm c} - \tau_1\right) dt. \quad (4)$$

The range of integration here is actually determined mathematically by the time interval over which the locally generated pulse $w_{\rm cor}(t - jT_{\rm f} - c_i^{(1)}T_{\rm c} - \tau_1)$ is nonzero. The expression $x_j(u)$ can be simplified to

$$x_j(u) = A_1 s_j^{(1)}(u) + \underbrace{\sum_{k=2}^{N_{\rm u}} A_k s_j^{(k)}(u) \; + \; n_j(u)}_{\triangleq n(u)} \quad (5)$$

where $s_j^{(k)}(u)$ is evaluated in Appendix I as

$$s_j^{(k)}(u) = \tilde{R}_w\left(\left[c_j^{(1)} - c_{j+j_{1,k}(u)}^{(k)}(u)\right]T_{\rm c} + d_{j+j_{1,k}(u)}^{(k)}(u) + \alpha_{1,k}(u)\right) \quad (6)$$

$$\tilde{R}_w(\tau) = \int_{-\infty}^{\infty} w_{\rm rec}(t+\tau) w_{\rm cor}(t)\, dt \quad (7)$$

$$j_{1,k}(u) = \left[\left[\frac{\tau_1 - \tau_k(u)}{T_{\rm f}}\right]\right] \quad (8)$$

$$\alpha_{1,k}(u) = \tau_1 - \tau_k(u) \bmod T_{\rm f}. \quad (9)$$

The notation $[[z]]$ represents z rounded to the nearest integer. Notice that $\tilde{R}_w(\tau)$ is the cross correlation between the received monocycle waveform and the signal $w_{\rm cor}(t)$ present at the output of the receiver template generator, and it is typically an odd function. Assuming that the monocycle waveforms $w_{\rm rec}(t)$ and $w_{\rm cor}(t)$ are nonzero only in the time interval $[0, T_{\rm m}]$, it follows that $\tilde{R}_w(\tau) = 0$ for $|\tau| > T_{\rm m}$. The quantity $n_j(u)$ is the component of $n(u,t)$ that affects the reception of signal 1, i.e.,

$$n_j(u) = \int_{-\infty}^{\infty} n(u,t) w_{\rm cor}\left(t - jT_{\rm f} - c_j^{(1)}T_{\rm c} - \tau_1\right) dt. \quad (10)$$

The desired signal sample has an especially simple form, namely

$$s_j^{(1)}(u) = \tilde{R}_w\left(d_j^{(1)}(u)\right) \approx \dot{\tilde{R}}_w(0) d_j^{(1)}(u) \quad (11)$$

where the latter approximation is valid when the data modulation $d_j^{(1)}(u)$ is constrained to be within the linear region of the $\tilde{R}_w(\cdot)$ function, and $\dot{\tilde{R}}_w(0)$ represents the slope of $\tilde{R}_w(t)$ at $t = 0$. Fig. 3 shows exact and approximate expressions for the cross-correlation function $\tilde{R}_w(\tau)$ for the typical received waveform given in Fig. 1. When the approximation is valid, the sampled modulation is directly visible at the correlator output with little or no distortion. Furthermore, since the modulation is highly oversampled to provide spread-spectrum processing gain, adjacent random variables in the desired signal sequence $\{s_j^{(1)}(u)\}$ are highly correlated.

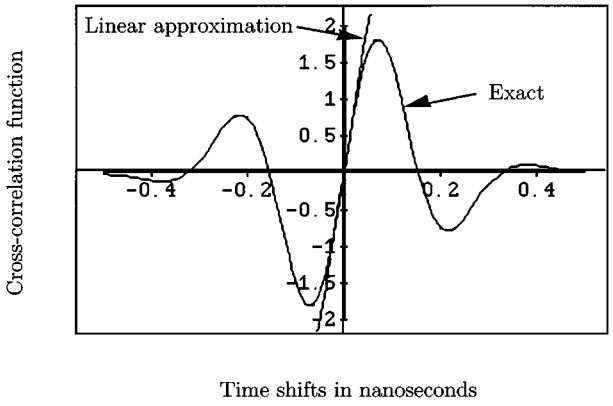

Fig. 3. Cross correlation $\tilde{R}_w(\tau)$ between the received waveform of Fig. 1 and the pulse correlator waveform $w_{\rm cor}(t)$ (chosen equal to $(d/dt)w_{\rm rcc}(t)$ of Fig. 1). In this example, the linear approximation (also shown) appears reasonable as long as $\tau \leq 0.03$ nanoseconds.

B. Subcarrier Demodulator Input Model

As indicated in Fig. 2, the impulse correlator output values are sampled to obtain the sequence $\{x_j(u)\}$ and held to create a signal

$$y(u,t) = \sum_{j=-\infty}^{\infty} x_j(u) \overline{|T_{\rm f}|}(t - jT_{\rm f} - \gamma) \quad (12)$$

where γ is a delay on the order of $\tau_1 + T_{\rm f}$, and the rectangle function is defined by

$$\overline{|T|}(t) \triangleq \begin{cases} 1, & \text{for } |t| < T/2 \\ 0, & \text{otherwise.} \end{cases} \tag{13}$$

This signal is passed through a subcarrier filter to produce the signal $z(u,t)$ that is to be demodulated.

The convolution integral representation of the output of the subcarrier filter with impulse response $g_{\rm subcar}(t)$ and input (12) can be used to obtain the output representation

$$z(u,t) = T_{\rm f} \sum_{j=-\infty}^{\infty} x_j(u) g'_{\rm subcar}(t - jT_{\rm f} - \gamma) \tag{14}$$

where $g'_{\rm subcar}(t) \triangleq (1/T_{\rm f}) \int_{-\infty}^{\infty} \overline{|T_{\rm f}|}(t') g_{\rm subcar}(t - t')\, dt'$. When $1/T_{\rm f}$ is much larger than any frequency passed by the subcarrier filter, then $g'_{\rm subcar}(t) \approx g_{\rm subcar}(t)$.

As for the case of the correlator output signal in (5), the subcarrier filter output signal $z(u,t)$ can be broken down into separate components in a similar fashion

$$z(u,t) = z^{(1)}(u,t) + \underbrace{\sum_{k=2}^{N_{\rm u}} z^{(k)}(u,t) + z_{\rm rec}(u,t)}_{\triangleq z_{\rm noisc}(u,t)} \tag{15}$$

where

$$z^{(k)}(u,t) = T_{\rm f} \sum_{j=-\infty}^{\infty} A_k s_j^{(k)}(u) g'_{\rm subcar}(t - jT_{\rm f} - \gamma) \tag{16}$$

and

$$z_{\rm rec}(u,t) = T_{\rm f} \sum_{j=-\infty}^{\infty} n_j(u) g'_{\rm subcar}(t - jT_{\rm f} - \gamma). \tag{17}$$

The component $z_{\rm rec}(u,t)$ of $z_{\rm noise}(u,t)$ accounts for receiver noise and all other non-monocycle interference.

Since the receiver correlation circuitry is set to receive the signal from transmitter 1, the components $z^{(k)}(u,t)$ for $k = 2, 3, \cdots, N_{\rm u}$ in (15) represent the interference due to multiple-access noise at the demodulator input. From (11) and (16), the desired input signal $z^{(1)}(u,t)$ to the demodulator can be written as

$$z^{(1)}(u,t) = T_{\rm f} A_1 \sum_{j=-\infty}^{\infty} \tilde{R}_w(d_j^{(1)}(u)) g'_{\rm subcar}(t - jT_{\rm f} - \gamma). \tag{18}$$

We assume for simplicity that perfect signal reconstruction from the samples takes place, i.e., $g'_{\rm subcar}(t)$ is an ideal interpolating function for reconstructing the waveform from samples. Under this assumption of perfect signal reconstruction $z^{(1)}(u,t)$ becomes

$$z^{(1)}(u,t) = A_1 \tilde{R}_w(d^{(1)}(u, t - \gamma')) \tag{19}$$

where $d^{(1)}(u,t)$ represents the desired subcarrier signal before sampling and γ' accounts for propagation and processing delays.

C. Single-User Signal-to-Noise Ratio (SNR) Calculations

The single-user synchronous SNR $\mathrm{SNR}_{\rm m}(1)$ for a single monocycle at the output of the correlator is

$$\mathrm{SNR}_{\rm m}(1) \triangleq \frac{\mathbb{E}\left\{ \left| A_1 s_j^{(1)}(u) \right|^2 \right\}}{\mathbb{E}\{|n_j(u)|^2\}}. \tag{20}$$

The numerator of the above expression can be rewritten using (11) as

$$\begin{aligned} \mathbb{E}\left\{ \left| A_1 s_j^{(1)}(u) \right|^2 \right\} &= \mathbb{E}\left\{ \left| A_1 \tilde{R}_w\left(d_j^{(1)}(u) \right) \right|^2 \right\} \\ &= A_1^2 R_{\rm subcar}(0) \end{aligned} \tag{21}$$

where $R_{\rm subcar}(0)$ is the correlation function of the process $\tilde{R}_w(d^{(1)}(u,t))$ evaluated at zero shift and is also the mean-squared value of $\tilde{R}_w(d_j^{(1)}(u))$. We assume in this analysis that the random sequence $\{n_j(u)\}$ is composed of independent random variables with zero mean and variance $\sigma_{\rm n}^2$. This is a reasonable model for wide-band interference and receiver noise. Then, using (21)

$$\mathrm{SNR}_{\rm m}(1) = \frac{A_1^2 R_{\rm subcar}(0)}{\sigma_{\rm n}^2}. \tag{22}$$

Notice that the stationarity assumption of $d^{(k)}(u,t)$ implies that $\mathrm{SNR}_{\rm m}(1)$ has the same value for all choices of j.

The single-user SNR at the output of the subcarrier filter is defined to be

$$\mathrm{SNR}_{\rm out}(1) \triangleq \frac{\left\langle \mathbb{E}\left\{ \left| z^{(1)}(u,t) \right|^2 \right\} \right\rangle}{\left\langle \mathbb{E}\left\{ \left| z_{\rm rec}(u,t) \right|^2 \right\} \right\rangle}. \tag{23}$$

The notation $\langle \cdot \rangle$ is used to indicate a time average, in this case over the duration $T_{\rm f}$ of the "hold," to make this measure insensitive to time, i.e.,

$$\left\langle \mathbb{E}\left\{ \left| z^{(1)}(u,t) \right|^2 \right\} \right\rangle \triangleq \frac{1}{T_{\rm f}} \int_0^{T_{\rm f}} \mathbb{E}\left\{ \left| z^{(1)}(u, t - \zeta) \right|^2 \right\} d\zeta. \tag{24}$$

Using (19), (24) reduces to

$$\begin{aligned} \left\langle \mathbb{E}\left\{ \left| z^{(1)}(u,t) \right|^2 \right\} \right\rangle &= \mathbb{E}\left\{ \left| A_1 \tilde{R}_w\left(d^{(1)}(u, t - \gamma') \right) \right|^2 \right\} \\ &= A_1^2 R_{\rm subcar}(0). \end{aligned} \tag{25}$$

The quantity $\langle \mathbb{E}\{|z_{\rm rec}(u,t)|^2\} \rangle$, the noise power at the output of the subcarrier filter due to receiver noise, is calculated in (68) of Appendix III. The filter used in this calculation is

$$G'_{\rm subcar}(f) \approx \begin{cases} 1, & f_{\rm sc} - B/2 < |f| < f_{\rm sc} + B/2 \\ 0, & \text{otherwise} \end{cases} \tag{26}$$

where B is a measure of the modulated subcarrier bandwidth and $f_{\rm sc}$ is the subcarrier frequency. Technically, since the bandwidth will be used in evaluating the noise power in the output, it should be equal to the noise equivalent bandwidth of the subcarrier filter $G'_{\rm subcar}(f)$.

Substituting (25) and (68) into (23) gives

$$\mathrm{SNR}_{\rm out}(1) = \frac{A_1^2 R_{\rm subcar}(0)}{2BT_{\rm f}\sigma_{\rm n}^2} = \frac{\mathrm{SNR}_{\rm m}(1)}{2BT_{\rm f}}. \tag{27}$$

Hence, $\mathrm{SNR}_{\rm out}(1)$ is proportional to $\mathrm{SNR}_{\rm m}(1)$ of (22) with the proportionality factor being, as expected, approximately the

ratio of the filter output bandwidth $(2B)$ to input bandwidth $(\approx 1/T_{\rm f})$.

D. Multiple-User Interference Calculation

To calculate the effect of multiple-user interference, two assumptions are made.

1) *Random Sequence Selection*: Assume a randomly chosen sequence signal-set model, in which the hopping sequence $\{c_j^{(k)}(u)\}$ of each user k is selected independently of the selection of other user sequences. This is a conservative assumption because one would expect to do somewhat better by selecting the sequences to minimally interfere with each other.
2) *Independent Interference Sources*: Assume that the signals $s_{\rm rec}^{(k)}(u, t-\tau_k(u))$, for $k=2,3,\cdots,N_{\rm u}$ and $n(u,t)$ are independently generated. Therefore, the received signals from different users are totally asynchronous, and the delay variables $\tau_k(u)$ are independent for different users. Furthermore, the intraframe delay variable $\alpha_{1,k}(u)$ and the frame delay variable $j_{1,k}(u)$ for each user are independent random variables. Hence, the $N_{\rm u}$ random variables $s_j^{(k)}(u)$, for $k=2,3,\cdots,N_{\rm u}$, and $n_j(u)$ are independent random variables.

The $N_{\rm u}$-user SNR for a single monocycle at the output of the correlator can be defined as

$$\mathrm{SNR}_{\rm m}(N_{\rm u}) \triangleq \frac{\mathbb{E}\left\{\left|A_1 s_j^{(1)}(u)\right|^2\right\}}{\mathbb{E}\left\{\left|n(u)\right|^2\right\}}. \tag{28}$$

The numerator of this expression is calculated in (21). It is shown in Appendix II that the random variables $s_j^{(k)}(u)$ for $k=2,3,\cdots,N_{\rm u}$ are zero mean. Therefore, each of the random variables in the expression $n(u)$ defined in (5) are independent with zero mean, and hence

$$\mathbb{E}\left\{\left|n(u)\right|^2\right\} = \sigma_{\rm n}^2 + \sigma_{\rm self}^2 \sum_{k=2}^{N_{\rm u}} A_k^2 \tag{29}$$

where $\sigma_{\rm self}^2$ is defined in (65) of Appendix II. Therefore

$$\mathrm{SNR}_{\rm m}(N_{\rm u}) = \frac{A_1^2 R_{\rm subcar}(0)}{\sigma_{\rm n}^2 + \sigma_{\rm self}^2 \sum_{k=2}^{N_{\rm u}} A_k^2}. \tag{30}$$

Note that when $N_{\rm u}=1$, the second term in the denominator of the above expression is zero, and (30) reduces to (22).

The $N_{\rm u}$-user SNR at the output of the subcarrier filter is

$$\mathrm{SNR}_{\rm out}(N_{\rm u}) \triangleq \frac{\left\langle \mathbb{E}\left\{\left|z^{(1)}(u,t)\right|^2\right\}\right\rangle}{\left\langle \mathbb{E}\left\{\left|z_{\rm noise}(u,t)\right|^2\right\}\right\rangle}. \tag{31}$$

The total noise power $\langle \mathbb{E}\{|z_{\rm noise}(u,t)|^2\}\rangle$ at the demodulator input is evaluated in (69) of Appendix III. Substituting (25) and (69) into (31) gives

$$\mathrm{SNR}_{\rm out}(N_{\rm u}) = \frac{A_1^2 R_{\rm subcar}(0)}{2BT_{\rm f}\sigma_{\rm n}^2 + 2BT_{\rm f}\sigma_{\rm self}^2 \sum_{k=2}^{N_{\rm u}} A_k^2}. \tag{32}$$

When $N_{\rm u}=1$, the second term in the denominator is zero and (32) is equivalent to (27).

IV. Digital Impulse Radio Multiple-Access Receiver (DIRMA)

A. Receiver Signal Processing

The DIRMA receiver is based on the theory of hypothesis testing for fully coherent data detection. The objective is to determine a reasonable model for the signal processing necessary to demodulate one symbol of the transmission from the first transmitter with binary modulation. Specifically, $d_j^{(k)}(u) = \delta D_{\lfloor j/N_{\rm s}\rfloor}^{(k)}(u)$ where the data sequence $\{D_i^{(k)}(u)\}_{i=-\infty}^{\infty}$ is a binary (0 or 1) symbol stream that conveys information in some form, and the parameter δ is on the order of $T_{\rm m}$. Since this is an oversampled modulation system with $N_{\rm s}$ monocycles transmitted per symbol, the modulating data symbol changes only every $N_{\rm s}$ hops. Assuming that a new data symbol begins with pulse index $j=0$, the index of the data symbol modulating pulse j is $\lfloor j/N_{\rm s}\rfloor$ (here, the notation $\lfloor x\rfloor$ denotes the integer part of x). In this modulation method, no additional time shift is modulated on the monocycle when the data symbol is 0, but a time shift of δ is added to a monocycle when the symbol is 1.

The DIRMA receiver must decide whether $D_0^{(1)}(u)$ is 0 or 1, based on an observation of the received signal $r(u,t)$ in a time interval of duration $T_{\rm s} = N_{\rm s}T_{\rm f}$ at the antenna terminals. This corresponds to deciding between two hypotheses $\mathcal{H}_0$ and $\mathcal{H}_1$, where

$$\mathcal{H}_d: \quad r(u,t) = A_1 \sum_{j=0}^{N_{\rm s}-1} w_{\rm rec}\Big(t - \tau_1 - jT_{\rm f} - c_j^{(1)}T_{\rm c} - \delta d\Big) + n_{\rm tot}(u,t) \tag{33}$$

in which d is either 0 or 1. The remaining signals, interference, and noise have been lumped into the waveform

$$n_{\rm tot}(u,t) = \underbrace{\sum_{k=2}^{N_{\rm u}} A_k s_{\rm rec}^{(k)}(u, t-\tau_k(u))}_{\text{multiple-access noise}} + \underbrace{n(u,t)}_{\text{receiver noise, etc.}}. \tag{34}$$

As with the analog impulse radio, it is assumed that the receiver has achieved perfect clock and sequence synchronization for the signal transmitted by the first transmitter.

If no other users were present, and if the data $\{D_i^{(1)}(u)\}$ was composed of independent random variables, then the optimum receiver is the correlation receiver [15]–[17], which can be reduced to (35), shown at the bottom of the page, where $v(t) \triangleq w_{\rm rec}(t) - w_{\rm rec}(t-\delta)$. Since $w_{\rm rec}(t)$ is nonzero only in the time interval $[0, T_{\rm m}]$, the support of $v(t)$ is $[0, T_{\rm m}+\delta]$. The statistic $\alpha(u)$ in (35) consists of summing the $N_{\rm s}$ correlations of the *correlator's template signal* $v(t)$ at various time shifts with the received signal $r(u,t)$. The signal processing corresponding to the decision rule (35) is shown in Fig. 4. A graph of the template signal is shown in Fig. 5 using the typical received waveform given in Fig. 1.

Strictly speaking, the above decision rule is no longer optimum when other users are present. In the presence of multiple-access noise, which is not really Gaussian, the optimum receiver makes use of the information that the receiver knows about the structure of the multiple-access noise. This optimal

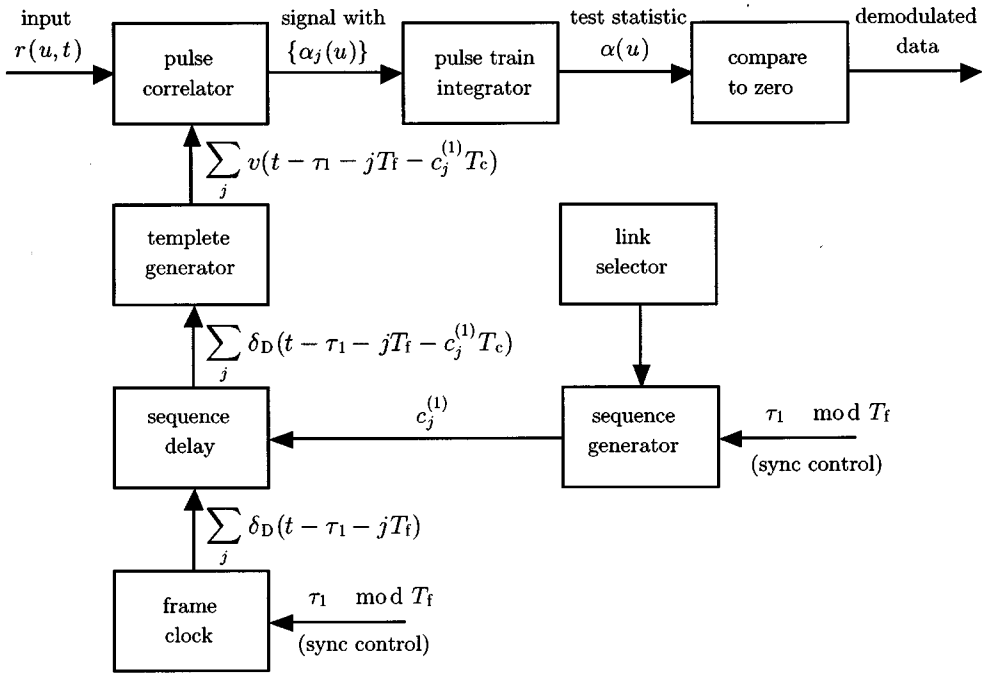

Fig. 4. Receiver block diagram for the reception of the first user's signal. Clock pulses are denoted by Dirac delta functions $\delta_{\rm D}(\cdot)$.

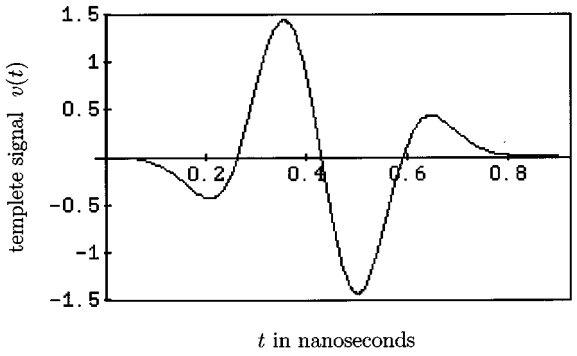

Fig. 5. The template signal $v(t)$ for the signal of Fig. 1. The parameter δ was chosen to be 0.156 nanoseconds in this example to approximately maximize $\mathrm{SNR}_{\rm out}(N_{\rm u})$. Since the template is the difference of two pulses shifted by δ, the nonzero extent of the template signal is approximately δ plus the pulsewidth, i.e., about 0.86 nanoseconds.

detection in a multiuser environment leads to much more complex receiver designs [18], [19]. However, if the number of users is large and no such multiuser detector is feasible, then it is reasonable to approximate the combined effect of the other users as a Gaussian random process [14]. Under this approximation, the total noise $n_{\rm tot}(u,t)$ is a spectrally white Gaussian random process and (35) is optimum. While the assumptions that make the rule (35) optimal are not strictly valid, this decision rule will be used in the following to evaluate the performance of the DIRMA receiver as a simple suboptimal means of making decisions because it is theoretically simple and suggests practical implementations.

The test statistic $\alpha(u)$ can be rewritten as

$$\alpha(u) = m + n_{\rm d}(u) \tag{36}$$

where the quantities m (under hypotheses $\mathcal{H}_1$) and $n_{\rm d}$ are given by

$$m = \sum_{j=0}^{N_s-1} \int_{\tau_1+jT_f}^{\tau_1+(j+1)T_f} \left[A_1 \sum_{i=0}^{N_s-1} w_{\rm rec}\left(t-\tau_1-iT_f-c_i^{(1)}T_c-\delta\right)\right] \times v\left(t-\tau_1-jT_f-c_j^{(1)}T_c\right) dt \tag{37}$$

and

$$n_{\rm d}(u) = \sum_{j=0}^{N_s-1} \int_{\tau_1+jT_f}^{\tau_1+(j+1)T_f} n_{\rm tot}(u,t) \times v\left(t-\tau_1-jT_f-c_j^{(1)}T_c\right) dt \tag{38}$$

respectively.

$$\text{``decide'' } D_0^{(1)} = 0'' \quad \Leftrightarrow \quad \underbrace{\sum_{j=0}^{N_s-1} \overbrace{\int_{\tau_1+jT_f}^{\tau_1+(j+1)T_f} r(u,t) v\left(t-\tau_1-jT_f-c_j^{(1)}T_c\right) dt}^{\text{pulse correlator output} \triangleq \alpha_j(u)} > 0}_{\text{test statistic} \triangleq \alpha(u)} \tag{35}$$

The quantity m is evaluated in Appendix IV as

$$m = N_{\rm s} A_1 m_{\rm p} \tag{39}$$

where $m_{\rm p}$ is defined in (71) of Appendix IV.

The expression in (38) is further simplified in Appendix V as

$$n_{\rm d}(u) = \sum_{k=2}^{N_{\rm u}} A_k n^{(k)}(u) + n_{\rm rec}(u) \tag{40}$$

where $n^{(k)}(u)$ is caused by multiple-access noise from the kth transmitter and $n_{\rm rec}(u)$ is caused by receiver noise and other sources of non-monocycle interference. Their mathematical expressions can be found in (76) and (74) of Appendix V.

B. SNR of the DIRMA Receiver

The DIRMA receiver output SNR is defined to be

$$\mathrm{SNR}_{\rm out}(N_{\rm u}) \triangleq \frac{m^2}{\mathbb{E}\left\{|n_{\rm d}(u)|^2\right\}} \tag{41}$$

where the numerator of this expression is given in (39). It is shown in Appendix VI that the random variables $n^{(k)}(u)$ for $k = 2, 3, \cdots, N_{\rm u}$ are zero mean. Since each of the random variables in the expression of $n_{\rm d}(u)$ defined in (40) are independent with zero mean, the quantity $\mathbb{E}\{|n_{\rm d}(u)|^2\}$ becomes

$$\mathbb{E}\left\{|n_{\rm d}(u)|^2\right\} = \sigma_{\rm rec}^2 + N_{\rm s}\sigma_{\rm a}^2 \sum_{k=2}^{N_{\rm u}} A_k^2. \tag{42}$$

The quantity $\sigma_{\rm rec}^2$ is the variance of the receiver noise component at the pulse train integrator output. The parameter $\sigma_{\rm a}^2$ is defined in (79) of Appendix VI.

When only the desired transmitter is on the air, $N_{\rm u} = 1$, and the single-user output SNR is

$$\mathrm{SNR}_{\rm out}(1) = \frac{(N_{\rm s} A_1 m_{\rm p})^2}{\sigma_{\rm rec}^2}. \tag{43}$$

Thus, $\mathrm{SNR}_{\rm out}(1)$ is equivalent to the output SNR that one might observe in single link experiments. This is a convenient parameter because it absorbs all of the scaling problems that one must confront in handling receiver noise and non-monocycle forms of interference. When more than one monocycle transmitter is on the air, then $\mathrm{SNR}_{\rm out}(N_{\rm u})$ can be written using (42) as

$$\mathrm{SNR}_{\rm out}(N_{\rm u}) = \frac{(N_{\rm s} A_1 m_{\rm p})^2}{\sigma_{\rm rec}^2 + N_{\rm s}\sigma_{\rm a}^2 \sum_{k=2}^{N_{\rm u}} A_k^2}. \tag{44}$$

When $N_{\rm u} = 1$, the second term in the denominator is zero and (44) is reduced exactly to the expression in (43).

V. Performance Measures of Multiple-Access Systems

A. Analog/Digital Comparisons

The similarity of the structure of $\mathrm{SNR}_{\rm out}(N_{\rm u})$ for analog and digital receivers given in (32) and (44) suggests a generalized expression of the form

$$\mathrm{SNR}_{\rm out}(N_{\rm u}) = \left\{ \mathrm{SNR}_{\rm out}^{-1}(1) + M \sum_{k=2}^{N_{\rm u}} \left(\frac{A_k}{A_1}\right)^2 \right\}^{-1}. \tag{45}$$

The $\mathrm{SNR}_{\rm out}^{-1}(1)$ for the AIRMA and DIRMA are given in (27) and (43), respectively. The values of M for the AIRMA and DIRMA receivers are given, respectively, by

$$\begin{aligned} M_{\rm AIRMA}^{-1} &\triangleq \frac{R_{\rm subcar}(0)}{2BT_{\rm f}\sigma_{\rm self}^2} \\ &= \frac{R_{\rm subcar}(0)}{R_{\rm Amod} T_{\rm f} \sigma_{\rm self}^2} \\ &= \frac{\tilde{M}_{\rm AIRMA}^{-1}}{R_{\rm Amod}} \end{aligned} \tag{46}$$

$$\begin{aligned} M_{\rm DIRMA}^{-1} &\triangleq \frac{N_{\rm s} m_p^2}{\sigma_{\rm a}^2} \\ &= \frac{m_p^2}{R_{\rm Dmod} T_{\rm f} \sigma_{\rm a}^2} \\ &= \frac{\tilde{M}_{\rm DIRMA}^{-1}}{R_{\rm Dmod}}. \end{aligned} \tag{47}$$

Because all measures of the communication rate are hidden in M, we have defined the rates of the analog and digital systems in (45) as $R_{\rm Amod} \triangleq 2B$ and $R_{\rm Dmod} \triangleq 1/N_{\rm s}T_{\rm f}$, respectively, and shown them explicitly in the modulation index expressions. The remaining factor in these expressions is denoted by $\tilde{M}$.

The general form of (45) was developed originally in [20] and was calculated specifically for a DS-CDMA system in [21]. Since $\mathrm{SNR}_{\rm out}(N_{\rm u})$ for the AIRMA and DIRMA are identical with the exception of different modulation coefficients $M_{\rm AIRMA}$ and $M_{\rm DIRMA}$, the achievable transmission rate and multiple-access capacity are derived for a general impulse radio with parameter M (without the subscripts). Then, performance comparisons of specific receivers are equivalent to comparisons of their modulation coefficients M.

The basic performance measures of multiple-access systems that we will relate are the number $N_{\rm u}$ of users, the operating SNR, $\mathrm{SNR}_{\rm out}(N_{\rm u})$ for $N_{\rm u}$ users, the modulation rate $R_{\rm mod}$, the modulation index $\tilde{M}$, and the excess single-link SNR $\Delta P \triangleq 10\log_{10}\{\mathrm{SNR}_{\rm out}(1)/\mathrm{SNR}_{\rm out}(N_{\rm u})\}$ required to support multiple-access operation for this number of users. In these terms, (45) reduces to

$$\sum_{k=2}^{N_{\rm u}} \left(\frac{A_k}{A_1}\right)^2 = \tilde{M}^{-1} R_{\rm mod}^{-1} \mathrm{SNR}_{\rm out}^{-1}(N_{\rm u}) \left\{1 - 10^{-(\Delta P/10)}\right\} \tag{48}$$

where $R_{\rm mod}$ is $R_{\rm Amod}$ for analog modulation or $R_{\rm Dmod}$ for digital modulation.

Under perfect power control assumptions, i.e., $A_k = A_1$ for all k, (48) yields simple relations between the parameters of interest as

$$\begin{aligned} R_{\rm mod}(\Delta P) = \tilde{M}^{-1} \mathrm{SNR}_{\rm out}^{-1}(N_{\rm u}) &\left\{1 - 10^{-(\Delta P/10)}\right\} \\ &\times \{N_{\rm u} - 1\}^{-1} \end{aligned} \tag{49}$$

$$N_{\rm u}(\Delta P) = \left\lfloor \tilde{M}^{-1} \mathrm{SNR}_{\rm out}^{-1}(N_{\rm u}) \left\{1 - 10^{-(\Delta P/10)}\right\} \right\rfloor + 1 \tag{50}$$

both monotonically increasing functions of ΔP. The ultimate limits to multiple-access communication with impulse radio

multiple-access receivers occur when ΔP is increased without bound, i.e.,

$$R_{\mathrm{mod}}(\Delta P) \le \lim_{\Delta P \to \infty} R_{\mathrm{mod}}(\Delta P) = \tilde{M}^{-1}\mathrm{SNR}_{\mathrm{out}}^{-1}(N_{\mathrm{u}})\{N_{\mathrm{u}}-1\}^{-1} \triangleq R_{\max} \quad (51)$$

$$N_{\mathrm{u}}(\Delta P) \le \lim_{\Delta P \to \infty} N_{\mathrm{u}}(\Delta P) = \left\lfloor M^{-1}\mathrm{SNR}_{\mathrm{out}}^{-1}(N_{\mathrm{u}}) \right\rfloor + 1 \triangleq N_{\max}. \quad (52)$$

Hence, for a specified level of performance as embodied in $\mathrm{SNR}_{\mathrm{out}}(N_{\mathrm{u}})$, there are upper bounds on the modulation rate (for a given number of users) and the number of users (for a given modulation rate) that cannot be exceeded by the impulse radio multiple-access receivers. Similar results for DS-CDMA system can be found in [21].

VI. Performance Comparisons and Conclusions

The performance of the impulse radio multiple-access receiver will be evaluated for the analog receiver in which the data signal is binary frequency-shift keyed (FSK) modulation on a subcarrier that is subsequently detected to produce a received bit stream, and for the fully digital receiver with pulse-position modulation (PPM) (as described in Section IV). The basic parameters used to provide numerical results are shown in Table I.

In the AIRMA example

$$d^{(k)}(u,t) = K\sum_{n} \overline{[T_{\mathrm{s}}]}(t-nT_{\mathrm{s}}) \times \cos[2\pi(f_{\mathrm{c}}+\Delta f_n(u))t + \theta(u)] \quad (53)$$

where the rectangle function is defined by (13). The scaling constant K is chosen such that the linear approximation in (11) is reasonable. The random variable $\theta(u)$ is uniformly distributed on the interval $[-\pi,\pi)$. In the case of binary FSK, the subcarrier frequency f_{c} is shifted by $\Delta f_n(u) = f_0$ or $\Delta f_n(u) = f_1$ depending upon whether the nth data symbol is zero or one, respectively. The frequencies for FSK signaling are chosen to insure orthogonal signaling, and performance evaluation of the data detection process is based on standard results [15]–[17]. The quantity $R_{\mathrm{subcar}}(0)$, the mean-squared value of $\tilde{R}_w(d_j^{(1)}(u))$, is given by (81) of Appendix VII.

In DIRMA receivers, the PPM modulation parameter δ, which affects the shape of the template signal $v(t)$, appears only in m_{p} and σ_{a}^2 implicitly and can be adjusted to maximize $\mathrm{SNR}_{\mathrm{out}}(N_{\mathrm{u}})$ under various conditions [14]. We have chosen the value of δ that is optimum when receiver noise dominates the multiple-access noise, e.g., when there is only one user or when there is a strong external interferer. In this case, it follows from (43) that the optimum choice of modulation parameter is the one that maximizes $|m_{\mathrm{p}}|$. On the other hand, when the receiver noise is negligible and $\mathrm{SNR}_{\mathrm{out}}(1)$ is nearly infinite, the optimum choice of δ suggested by (44) would be the one that maximizes $|m_{\mathrm{p}}|/\sigma_{\mathrm{a}}$. The optimizing values of δ for these two criteria are close in value and provide comparable performance.

Sample performance parameters for analog and digital radio implementations are summarized in Table II. The number of

TABLE I
Numerical Example of Impulse Radio Basic Operating Parameters

Name	Notation	Typical Values
Impulse Width Parameter	τ_{m}	0.2877 ns
Impulse Width	T_{m}	≈ 0.7 ns
Impulse Repetition Frequency	T_{f}^{-1}	10 MHz
Frame Time	T_{f}	100 ns
Transmission Rate	R_{s}	19.2 Kbps
Symbol Time	$T_{\mathrm{s}} = R_{\mathrm{s}}^{-1}$	52.083 μs
Number of Impulses per Symbol	$T_{\mathrm{s}}T_{\mathrm{f}}^{-1}$	520.83

TABLE II
Sample Performance Parameters for Analog and Digital Radio Implementations

Parameter		AIRMA	DIRMA
Modulation Format		FSK on subcarrier	BPPM
Modulation Parameters		$\tilde{\tilde{R}}(0) = 40.9488$ $K = 0.025$ $\frac{1}{2}(\tilde{\tilde{R}}(0)K)^2 = 0.524$ $\sigma_{\mathrm{self}}^2 = 0.005898$ $\frac{(\tilde{\tilde{R}}(0)K)^2}{2\sigma_{\mathrm{self}}^2} = 88.8439$	 $\delta = 0.156$ ns $m_{\mathrm{p}}^2 = 0.0305$ $\sigma_{\mathrm{a}}^2 = 0.006045$ $\frac{m_{\mathrm{p}}^2}{\sigma_{\mathrm{a}}^2} \approx 504$
$\widetilde{M}^{-1}$		8.88×10^8	5.04×10^9
M^{-1} for $R_{\mathrm{s}} = 19.2$ Kbps		4.63×10^4	2.63×10^5
$N_{\max}$ for $R_{\mathrm{s}} = 19.2$ Kbps	at BER $= 10^{-3}$	4846	27488
	at BER $= 10^{-4}$	3353	19017
	at BER $= 10^{-5}$	2544	14426
$R_{\max}$ for 49 users	at BER $= 10^{-3}$	1.6 Mbps	9.1 Mbps
	at BER $= 10^{-4}$	1.09 Mbps	6.29 Mbps
	at BER $= 10^{-5}$	0.842 Mbps	4.77 Mbps

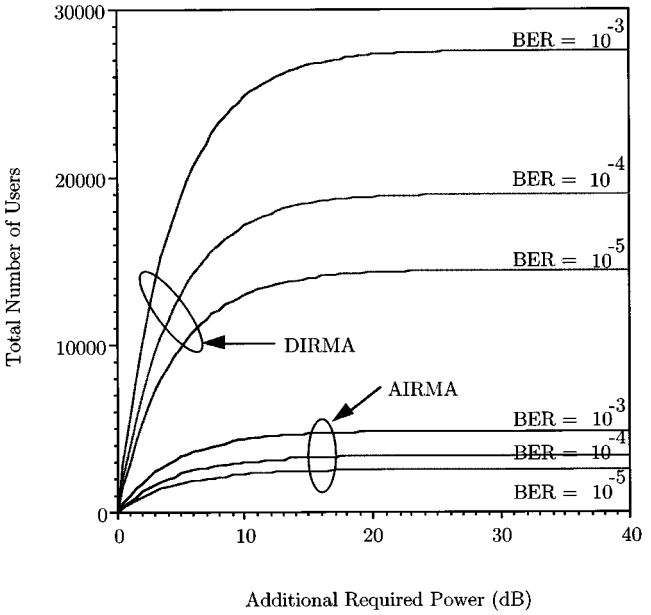

Fig. 6. Total number of users versus additional required power (decibels) for AIRMA and DIRMA receivers. This figure is plotted for three different performance levels with the data rate of 19.2 kb/s.

users versus additional required power for AIRMA and DIRMA receivers in an ideal additive white Gaussian noise (AWGN) power-controlled channel are plotted in Fig. 6 for typical bit-error rates. It is clear that the DIRMA receiver, which has been optimized for digital transmission, outperforms the AIRMA receiver, which is given the task of transporting a subcarrier with binary digital modulation. This follows from the fact that in the digital receiver each transmitted monocycle provides maximum discrimination between the two digital hypotheses that the receiver must test, while in the analog design, the constraint of maintaining linearity in the receiver reduces the effectiveness of the digital subcarrier detector. This comparison emphasizes the fact that the AIRMA design is meant for truly analog data waveforms.

Aside from these differences, it is interesting to note the large numbers of users both of these systems can support in an ideal power-controlled AWGN environment. These predictions are simply a result of the bandwidth that this signaling technology occupies in an ideal power-controlled aggregate AWGN channel.

Appendix I
Correlator Output Evaluation

By substituting the expression $s_{\rm rec}^{(k)}(u, t-\tau_k(u))$ in place of $r(u,t)$ in (4), the random signal variable $s_j^{(k)}(u)$ can be rewritten as a function of the TH sequences and the monocycle cross correlation $\tilde{R}_w(\tau)$ as

$$s_j^{(k)}(u) = \sum_{j'=-\infty}^{\infty} \tilde{R}_w\left([j-j']T_{\rm f} + \left[c_j^{(1)} - c_{j'}^{(k)}(u)\right]T_{\rm c} + d_{j'}^{(k)}(u) + [\tau_1 - \tau_k(u)]\right) \quad (54)$$

where $\tilde{R}_w(\tau)$ was defined in (7). Since $T_{\rm m} \ll T_{\rm f}$, only one term from the sum in (54) can be nonzero. There are two large time uncertainties in the argument of $\tilde{R}_w(\cdot)$ in (54), namely the transmission reference times τ_1 and $\tau_k(u)$ (see Fig. 7). Since these are related to the times when the radios begin transmission in asynchronous operation, the uncertainty concerning their difference may span *many* frame times $T_{\rm f}$. This difference can be modeled as

$$\tau_1 - \tau_k(u) = j_{1,k}(u)T_{\rm f} + \alpha_{1,k}(u), \qquad -T_{\rm f}/2 \le \alpha_{1,k}(u) < T_{\rm f}/2. \quad (55)$$

Here, $j_{1,k}(u)$ is the value of the time uncertainty $\tau_1 - \tau_k(u)$ rounded to the nearest frame time, and $\alpha_{1,k}(u)$ is the error in this rounding process. The argument of $\tilde{R}_w(\cdot)$ can be rewritten using (55) as

$$[j-j'+j_{1,k}(u)]T_{\rm f} + \underbrace{\overbrace{\left[c_j^{(1)} - c_{j'}^{(k)}(u)\right]T_{\rm c}}^{\text{magnitude}\le N_{\rm h}T_{\rm c}} + \overbrace{d_{j'}^{(k)}(u)}^{\text{magnitude}\le T_{\rm m}} + \overbrace{\alpha_{1,k}(u)}^{\text{magnitude}\le T_{\rm f}/2}}_{\text{magnitude}\le T_{\rm f}/2 + N_{\rm h}T_{\rm c} + T_{\rm m}}. \quad (56)$$

Assume for analytical convenience that the time interval over which the monocycle can be time-hopped is less than half a frame time so that

$$N_{\rm h}T_{\rm c} < T_{\rm f}/2 - 2T_{\rm m}. \quad (57)$$

This implies that $|[c_j^{(1)} - c_{j'}^{(k)}(u)]T_{\rm c} + d_{j'}^{(k)}(u) + \alpha_{1,k}(u)| < T_{\rm f} - T_{\rm m}$, and (54) becomes

$$s_j^{(k)}(u) = \sum_{j'=-\infty}^{\infty} \tilde{R}_w\Bigg([j-j'+j_{1,k}(u)]T_{\rm f} + \underbrace{\left[c_j^{(1)} - c_{j'}^{(k)}(u)\right]T_{\rm c} + d_{j'}^{(k)}(u) + \alpha_{1,k}(u)}_{\text{magnitude}<T_{\rm f}-T_{\rm m}}\Bigg). \quad (58)$$

Since $\tilde{R}_w(\tau)$ is nonzero only for $|\tau| < T_{\rm m}$, (58) is zero unless $j - j' + j_{1,k}(u) = 0$. Therefore

$$s_j^{(k)}(u) = \tilde{R}_w\left(\left[c_j^{(1)} - c_{j+j_{1,k}(u)}^{(k)}(u)\right]T_{\rm c} + d_{j+j_{1,k}(u)}^{(k)}(u) + \alpha_{1,k}(u)\right). \quad (59)$$

On the other hand, if (57) is not satisfied, then the representation of $s_j^{(k)}(u)$ above may contain more than one term, with the actual values depending on the involved random variables.

Appendix II
Evaluation of the Moments of $s_j^{(k)}(u)$

Since the intraframe delay variable $\alpha_{1,k}(u)$ is a round-off error of a large random variable $\tau_1 - \tau_k(u)$ [see (55)], it is reasonable to assume that $\alpha_{1,k}(u)$ is uniformly distributed over its range. Therefore, the probability density of $\alpha_{1,k}(u)$ for $k = 2, 3, \cdots, N_{\rm u}$ is

$$p_{\alpha_{1,k}(u)}(z) = \begin{cases} T_{\rm f}^{-1}, & -T_{\rm f}/2 \le z < T_{\rm f}/2 \\ 0, & \text{otherwise.} \end{cases} \quad (60)$$

The first moment of $s_j^{(k)}(u)$ for each of $k = 2, 3, \cdots, N_{\rm u}$ is calculated in two steps by first computing the conditional expectation over $\alpha_{1,k}(u)$, given the sequence variables and sampled-data variable, and then averaging over the sequence variables and sampled-data variable. By direct substitution of (59), it is easy to verify via the change of variable technique that the conditional expectation over $\alpha_{1,k}(u)$ is

$$\mathbb{E}_\alpha\left\{s_j^{(k)}(u)\right\} = T_{\rm f}^{-1}\int_{-T_{\rm f}/2+\left[c_j^{(1)}-c_{j+j_{1,k}(u)}^{(k)}(u)\right]T_{\rm c}+d_{j+j_{1,k}(u)}^{(k)}(u)}^{+T_{\rm f}/2+\left[c_j^{(1)}-c_{j+j_{1,k}(u)}^{(k)}(u)\right]T_{\rm c}+d_{j+j_{1,k}(u)}^{(k)}(u)} \cdot \tilde{R}_w(\zeta')\,d\zeta'. \quad (61)$$

Recall that $\tilde{R}_w(\tau) \neq 0$ only for $|\tau| \le T_{\rm m}$. Furthermore, the constraint (57) on $N_{\rm h}T_{\rm c}$ guarantees that the interval where $\tilde{R}_w(\tau)$ is nonzero is contained fully within the region of integration, regardless of the sequence element values and sample data value. Because of propagation effects, $\tilde{R}_w(t)$ generally is the derivative of a function that begins and ends at zero, implying that $\int_{-\infty}^{\infty} \tilde{R}_w(\tau)\,d\tau = 0$, the conditional expectation over $\alpha_{1,k}(u)$ in (61) is zero, and therefore

$$\mathbb{E}\left\{s_j^{(k)}(u)\right\} = 0, \qquad \text{for } k = 2, 3, \cdots, N_{\rm u}. \quad (62)$$

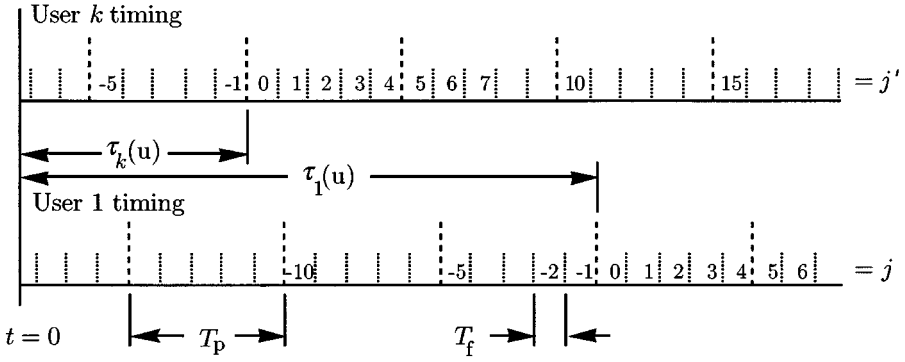

Fig. 7. Timing diagram, illustrating epochs and indexes for the signals received from user 1 and user k, with $N_p = 5$ (for this illustration only). The indexing begins from the zero reference time of the each users.

The second moment of $s_j^{(k)}(u)$ for each of $k = 2, 3, \cdots, N_u$ is calculated similarly and averaging over $\alpha_{1,k}(u)$ again is enough to complete the calculation of the second moment of $s_j^{(k)}(u)$. It can be shown that the conditional expectation of $|s_j^{(k)}(u)|^2$ over $\alpha_{1,k}(u)$ is

$$\mathbb{E}_\alpha\left\{\left|s_j^{(k)}(u)\right|^2\right\} = T_f^{-1}\int_{-T_f/2+\left[c_j^{(1)}-c^{(k)}_{j+j_{1,k}(u)}(u)\right]T_c+d^{(k)}_{j+j_{1,k}(u)}(u)}^{+T_f/2+\left[c_j^{(1)}-c^{(k)}_{j+j_{1,k}(u)}(u)\right]T_c+d^{(k)}_{j+j_{1,k}(u)}(u)} \cdot\left|\tilde{R}_w(\zeta')\right|^2 d\zeta'. \tag{63}$$

The domain of the above integral can be extended to cover the whole real line, and the conditional expectation of $|s_j^{(k)}(u)|^2$ over $\alpha_{1,k}(u)$ does not depend on the sequence variables and sampled-data variable. Therefore, using (7)

$$\mathbb{E}\left\{\left|s_j^{(k)}(u)\right|^2\right\} = \mathbb{E}_\alpha\left\{\left|s_j^{(k)}(u)\right|^2\right\} = T_f^{-1}\int_{-\infty}^{+\infty}\left|\tilde{R}_w(\tau)\right|^2 d\tau \tag{64}$$

$$= T_f^{-1}\int_{-\infty}^{\infty}\left[\int_{-\infty}^{\infty} w_{rec}(t+\tau)w_c(t)\,dt\right]^2 d\tau \triangleq \sigma^2_{self}. \tag{65}$$

The quantity $\mathbb{E}\{|s_j^{(k)}(u)|^2\}$ enters into the self-interference terms in the signal-to-noise calculations and has been named σ^2_{self}.

Appendix III
Evaluation of the Moments of the Demodulator Input Noise

The total noise at the demodulator input is composed of N_u independently generated components and is defined by (15). Now that it has been verified that $\mathbb{E}\{s_j^{(k)}(u)\} = 0$ and $\mathbb{E}\{n_j(u)\} = 0$, it follows immediately that:

$$\mathbb{E}\{z^{(k)}(u,t)\} = 0, \qquad k = 2, 3, \cdots, N_u$$
$$\mathbb{E}\{z_{rec}(u,t)\} = 0. \tag{66}$$

The mean-squared value of each of these random processes $z^{(k)}(u,t)$ is a straight-forward evaluation which is annotated as follows:

$$\begin{aligned}\left\langle\mathbb{E}\left\{|z_k(u,t)|^2\right\}\right\rangle &\overset{(a)}{=} (T_f A_k)^2\sum_{j=-\infty}^{\infty}\mathbb{E}\left\{\left|s_j^{(k)}(u)\right|^2\right\}\\ &\quad\times\left\langle|g'_{subcar}(t-jT_f-\gamma)|^2\right\rangle\\ &\overset{(b)}{=} (T_f A_k)^2\sigma^2_{self}\sum_{j=-\infty}^{\infty}\frac{1}{T_f}\\ &\quad\times\int_0^{T_f}|g'_{subcar}(t-jT_f-\gamma-\zeta)|^2\,d\zeta\\ &\overset{(c)}{=} T_f A_k^2\sigma^2_{self}\int_{-\infty}^{\infty}|g'_{subcar}(t)|^2\,dt\\ &\overset{(d)}{=} T_f A_k^2\sigma^2_{self}\int_{-\infty}^{\infty}|G'_{subcar}(f)|^2\,df\\ &\overset{(e)}{=} 2BT_f\sigma^2_{self}A_k^2.\end{aligned} \tag{67}$$

Here, (a) is the result of substituting the representation (16) of $z^{(k)}(u,t)$ and uses the fact that the variables in $\{s_j^{(k)}(u)\}$ are uncorrelated with zero mean, (b) substitutes the self interference notation and the definition of the time average given in (24), (c) converts the infinite collection of contiguous finite-domain integrals into a single integral, (d) uses Parseval's theorem for Fourier transforms, and (e) substitutes (26) and completes the integration.

Using the fact that the variables in $\{n_j(u)\}$ are uncorrelated with zero mean, the mean-squared value of the receiver noise $z_{rec}(u,t)$ can be calculated similarly to the calculation of (67) as

$$\left\langle\mathbb{E}\left\{|z_{rec}(u,t)|^2\right\}\right\rangle = 2BT_f\sigma_n^2. \tag{68}$$

Since the N_u components of $z_{noise}(u,t)$ are all mean-zero and independently generated, the total noise power into the subcarrier demodulator can now be reduced to

$$\left\langle\mathbb{E}\left\{|z_{noise}(u,t)|^2\right\}\right\rangle = 2BT_f\sigma_n^2 + 2BT_f\sigma^2_{self}\sum_{k=2}^{N_u}A_k^2. \tag{69}$$

APPENDIX IV
EVALUATION OF THE CONSTANT m

By the change of variables technique, the quantity in (39) can be rewritten as

$$m=\sum_{j=0}^{N_{\rm s}-1}\int_{-c_j^{(1)}T_{\rm c}}^{-c_j^{(1)}T_{\rm c}+T_{\rm f}}\left[A_1\sum_{i=0}^{N_{\rm s}-1}w_{\rm rec}\left(x+(j-i)T_{\rm f}+\left[c_j^{(1)}-c_i^{(1)}\right]T_{\rm c}-\delta\right)\right]v(x)\,dx. \quad (70)$$

But the support of $w_{\rm rec}(x+(j-i)T_{\rm f}+[c_j^{(1)}-c_i^{(1)}]T_{\rm c}-\delta)$ and the support of $v(x)$ overlap only if $i=j$. Therefore, $m=N_{\rm s}A_1m_{\rm p}$, where

$$m_{\rm p}\triangleq\int_{-\infty}^{\infty}w_{\rm rec}(x-\delta)v(x)\,dx. \quad (71)$$

APPENDIX V
EVALUATION OF $n_{\rm d}(u)$

Substitution of (34) for $n_{\rm tot}$ into (38) gives

$$n_{\rm d}(u)=\sum_{k=2}^{N_{\rm u}}A_kn^{(k)}(u)+n_{\rm rec}(u) \quad (72)$$

where $n^{(k)}(u)$ is the component of $n_{\rm d}(u)$ caused by multiple-access noise from the kth transmitter, i.e.,

$$n^{(k)}(u)=\sum_{j=0}^{N_{\rm s}-1}\int_{\tau_1+jT_{\rm f}}^{\tau_1+(j+1)T_{\rm f}}s_{\rm rec}^{(k)}(u,t-\tau_k(u))\times v\left(t-\tau_1-jT_{\rm f}-c_j^{(1)}T_{\rm c}\right)dt \quad (73)$$

$k=2,\cdots,N_{\rm u}$, and $n_{\rm rec}(u)$ is the component of $n_{\rm d}(u)$ that is caused by receiver noise and other sources of non-monocycle interference, i.e.,

$$n_{\rm rec}(u)=\sum_{j=0}^{N_{\rm s}-1}\int_{\tau_1+jT_{\rm f}}^{\tau_1+(j+1)T_{\rm f}}n(u,t)\times v\left(t-\tau_1-jT_{\rm f}-c_j^{(1)}T_{\rm c}\right)dt. \quad (74)$$

It is assumed that mean and variance of $n_{\rm rec}(u)$ are given by 0 and $\sigma_{\rm rec}^2$, respectively.

By the change of variables of integration and using the fact that the support of $v(\cdot)$ is contained in the region of integration, the quantity $n^{(k)}(u)$ can be reduced to

$$n^{(k)}(u)=\sum_{j=0}^{N_{\rm s}-1}\int_{-\infty}^{\infty}\left[\sum_{i=-\infty}^{\infty}w_{\rm rec}\left(x-\tau_k(u)+\tau_1+jT_{\rm f}+\left[c_j^{(1)}-c_i^{(k)}(u)\right]T_{\rm c}-iT_{\rm f}\delta d^{(k)}_{\lfloor i/N_{\rm s}\rfloor}(u)\right)\right]\times v(x)\,dx. \quad (75)$$

Using steps similar to (55)–(57) of Appendix I, the relative time shifts appearing in the argument of $w_{\rm rec}(\cdot)$ and $v(\cdot)$ can be bounded to show that only one term in the sum over i in (75) with index $i=j+j_{1,k}(u)$ is nonzero. Therefore, $n^{(k)}(u)$ simplifies to (76), shown at the bottom of the page.

APPENDIX VI
EVALUATION OF THE MOMENTS OF $n^{(k)}(u)$

Similar to the calculation of the first moment of $s_j^{(k)}(u)$ in Appendix II, it can be shown that $\mathbb{E}\{n_{kj}(u)\}=0$. Therefore, the first moment of $n^{(k)}(u)$ is

$$\mathbb{E}\left\{n^{(k)}(u)\right\}=\sum_{j=0}^{N_{\rm s}-1}\mathbb{E}\left\{n_{kj}(u)\right\}=0,\quad \text{for } k=2,3,\cdots,N_{\rm u}. \quad (77)$$

The second moment of $n^{(k)}(u)$ is

$$\mathbb{E}\left\{\left|n^{(k)}(u)\right|^2\right\}=\sum_{i=0}^{N_{\rm s}-1}\sum_{j=0}^{N_{\rm s}-1}\mathbb{E}\left\{n_{ki}^*(u)n_{kj}(u)\right\}=\sum_{i=0}^{N_{\rm s}-1}\mathbb{E}\left\{|n_{ki}(u)|^2\right\}+\sum_{i\neq j}\underbrace{\mathbb{E}\left\{n_{ki}^*(u)n_{kj}(u)\right\}}_{\triangleq\sigma_{\rm c}^2}. \quad (78)$$

The first term in the above equation can be calculated similar to the calculation of $\mathbb{E}\{|s_j^{(k)}(u)|^2\}$ in (65) in Appendix II as

$$\mathbb{E}\left\{|n_{ki}(u)|^2\right\}=T_{\rm f}^{-1}\int_{-\infty}^{\infty}\left[\int_{-\infty}^{\infty}w_{\rm rec}(x-s)\,v(x)\,dx\right]^2ds\triangleq\sigma_{\rm a}^2. \quad (79)$$

$$n^{(k)}(u)=\sum_{j=0}^{N_{\rm s}-1}\times\underbrace{\int_{-\infty}^{\infty}w_{\rm rec}\left(x+\alpha_{1,k}(u)+\left[c_j^{(1)}-c^{(k)}_{j+j_{1,k}(u)}(u)\right]T_{\rm c}-\delta d^{(k)}_{\lfloor j+j_{1,k}(u)/N_{\rm s}\rfloor}(u)\right)v(x)\,dx}_{\triangleq n_{kj}(u)}. \quad (76)$$

For the basic impulse radio operating parameters of interest, it can be verified numerically that $\sigma_{\rm a}^2 \gg (N_{\rm s}-1)\sigma_{\rm c}^2$. Therefore $\sigma_{\rm c}^2 \approx 0$, and hence $\mathbb{E}\{|n^{(k)}(u)|^2\} = N_{\rm s}\sigma_{\rm a}^2$.

APPENDIX VII
EVALUATION OF THE MEAN-SQUARED VALUE OF $\tilde{R}_w(d_j^{(k)}(u))$

The mean-squared value of $\tilde{R}_w(d_j^{(k)}(u))$ can be calculated as

$$\begin{aligned} R_{\rm subcar}(0) &= \mathbb{E}\left\{\left|\tilde{R}_w\left(d^{(k)}(u,t)\right)\right|^2\right\} \\ &= \mathbb{E}\left\{\left|\tilde{R}_w\left(d_j^{(k)}(u)\right)\right|^2\right\} \\ &\approx \mathbb{E}\left\{\left|\dot{\tilde{R}}(0)d^{(k)}(u,t)\right|^2\right\} \\ &\qquad \text{for small values of } d^{(k)}(u,t). \end{aligned} \quad (80)$$

For the analog FSK data subcarrier given in (53) and using the fact that $\overline{|T_{\rm s}|}(t-nT_{\rm s})\overline{|T_{\rm s}|}(t-mT_{\rm s}) = 0,\ \forall n \neq m, R_{\rm subcar}(0)$ can be reduced to

$$R_{\rm subcar}(0) = \frac{1}{2}(\dot{\tilde{R}}(0)K)^2 \underbrace{\sum_n \overline{|T_{\rm s}|}^2(t-nT_{\rm s})}_{=1} = \frac{1}{2}(\dot{\tilde{R}}(0)K)^2. \quad (81)$$

ACKNOWLEDGMENT

The authors would like to thank G. Chrisikos, R. J.-M. Cramer, L. D. Garrett, A. M. Petroff, L. W. Fullerton, and P. Withington for their encouragement and for several stimulating and helpful discussions.

REFERENCES

[1] R. A. Scholtz, "The spread-spectrum concept," *IEEE Trans. Commun.*, vol. COM-25, pp. 748–755, Aug. 1977.
[2] R. L. Pickholtz, D. L. Schilling, and L. B. Milstein, "Theory of spread-spectrum communications—A tutorial," *IEEE Trans. Commun.*, vol. COM-30, pp. 855–884, May 1982.
[3] M. K. Simon, J. K. Omura, R. A. Scholtz, and B. K. Levitt, *Spread Spectrum Communications Handbook*, revised ed. New York: McGraw-Hill, 1994.
[4] R. L. Peterson, R. E. Ziemer, and D. E. Borth, *Introduction to Spread Spectrum Communications*, 1st ed. Englewood Cliffs, NJ: Prentice Hall, 1995.
[5] M. Z. Win, R. A. Scholtz, and M. A. Barnes, "Ultra-wide bandwidth signal propagation for indoor wireless communications," in *Proc. IEEE Int. Conf. Communications*, vol. 1, Montréal, Canada, June 1997, pp. 56–60.
[6] M. Z. Win and R. A. Scholtz, "On the robustness of ultra-wide bandwidth signals in dense multipath environments," *IEEE Commun. Lett.*, vol. 2, pp. 51–53, Feb. 1998.
[7] G. F. Ross, "The transient analysis of certain TEM mode four-post networks," *IEEE Trans. Microwave Theory Tech.*, vol. MTT-14, p. 528, Nov. 1966.
[8] C. L. Bennett and G. F. Ross, "Time-domain electromagnetics and its applications," *Proc. IEEE*, vol. 66, pp. 299–318, Mar. 1978.
[9] M. Z. Win and R. A. Scholtz, "Energy capture vs. correlator resources in ultra-wide bandwidth indoor wireless communications channels," in *Proc. Military Communications Conf.*, vol. 3, Monterey, CA, Nov. 1997, pp. 1277–1281.
[10] M. Z. Win and R. A. Scholtz, "On the energy capture of ultra-wide bandwidth signals in dense multipath environments," *IEEE Commun. Lett.*, vol. 2, pp. 245–247, Sept. 1998.
[11] F. Ramírez-Mireles, M. Z. Win, and R. A. Scholtz, "Performance of ultra-wideband time-shift-modulated signals in the indoor wireless impulse radio channel," in *Proc. 31st Asilomar Conf. Signals, Systems and Computers*, Pacific Grove, CA, Nov. 1997, pp. 192–196.
[12] M. Z. Win and R. A. Scholtz, "Infinite Rake and selective Rake receivers for ultra-wide bandwidth transmissions in multipath environments," IEEE Commun. Lett., to be published.
[13] N. M. Abramson, "VSAT data networks," *Proc. IEEE*, vol. 78, pp. 1267–1274, July 1990.
[14] R. A. Scholtz, "Multiple access with time-hopping impulse modulation," in *Proc. Military Communications Conf.*, vol. 2, Boston, MA, Oct. 1993, pp. 447–450.
[15] J. M. Wozencraft and I. M. Jacobs, *Principles of Communication Engineering*, 1st ed, London, U.K.: Wiley, 1965.
[16] M. K. Simon, S. M. Hinedi, and W. C. Lindsey, *Digital Communication Techniques: Signal Design and Detection*, 1st ed. Englewood Cliffs, NJ: Prentice Hall, 1995.
[17] J. G. Proakis, *Digital Communications*, 3rd ed. New York: McGraw-Hill, 1995.
[18] H. V. Poor, "Signal processing for wideband communications," *IEEE Information Theory Society Newsletter*, June 1992.
[19] S. Verdu, "Recent progress in multiuser detection," in *Multiple Access Communications: Foundations for Emerging Technologies*. Piscataway, NJ: IEEE Press, 1993, pp. 164–175.
[20] G. R. Cooper and R. W. Nettleton, "A spread spectrum technique for high-capacity mobile communications," *IEEE Trans. Veh. Technol.*, vol. VT-27, pp. 264–275, Nov. 1978.
[21] C. L. Weber, G. K. Huth, and B. H. Batson, "Performance considerations of code division multiple-access systems," *IEEE Trans. Veh. Technol.*, vol. VT-30, pp. 3–9, Feb. 1981.

Moe Z. Win (S'85–M'87–SM'97) received the B.S. degree (magna cum laude) from Texas A&M University, College Station, and the M.S. degree from the University of Southern California (USC), Los Angeles, in 1987 and 1998, respectively, in electrical engineering. As a Presidential Fellow at USC, he received both the M.S. degree in applied mathematics and the Ph.D. degree in electrical engineering in 1998.

In 1987, he joined the Jet Propulsion Laboratory (JPL), California Institute of Technology, Pasadena. From 1994 to 1997, he was a Research Assistant with the Communication Sciences Institute, where he played a key role in the successful creation of the Ultra-Wideband Radio Laboratory at USC. Since 1998, he has been with the Wireless Systems Research Department, AT&T Laboratories-Research, Red Bank, NJ, as a Senior Technical Staff Member. His main research interests include the application of communication, detection, and estimation theories to a variety of communications problems including time-varying channels, diversity, equalization, synchronization, signal design, and ultrawide-bandwidth communication.

Dr. Win is a member of Eta Kappa Nu, Tau Beta Pi, Pi Mu Epsilon, Phi Theta Kappa, and Phi Kappa Phi. He was a University Undergraduate Fellow at Texas A&M University, where he received, among others awards, the Academic Excellence Award. At USC, he received several awards including the Outstanding Research Paper Award and the Phi Kappa Phi Student Recognition Award. He was the recipient of the IEEE Communications Society Best Student Paper Award at the Fourth Annual IEEE NetWorld+Interop'97 Conference. He has been involved in chairing and organizing sessions in a number of IEEE conferences. He served as a member of the Technical Program Committee for the IEEE Communication Theory Symposium during GLOBECOM'99, the 1999 IEEE Wireless Communications and Networking Conference, and the 1999 IEEE 49th Annual International Vehicular Technology Conference. He has also served as a member of the International Advisory Committee for the 1999 IEEE 50th International Vehicular Technology Conference. He currently serves as the Tutorial Chair for the 2001 IEEE International Vehicular Technology Conference and the Technical Program Chair for the IEEE Communication Theory Symposium during GLOBECOM 2000. Currently, he is the Editor for *Equalization and Diversity* for the IEEE TRANSACTIONS ON COMMUNICATIONS.

Robert A. Scholtz (S'56–M'59–SM'73–F'80) was born in Lebanon, OH, on January 26, 1936. He is a Distinguished Alumnus of the University of Cincinnati, Cincinnati, OH, where, as a Sheffield Scholar, he received the B.S. degree in electrical engineering in 1958. He was a Hughes Masters and Doctoral Fellow while obtaining the M.S. and Ph.D. degrees in electrical engineering from the University of California (USC), Los Angeles, and Stanford University, Stanford, CA, in 1960 and 1964, respectively.

While working on missile radar signal processing problems, he remained part-time at Hughes Aircraft Company from 1963 to 1978. In 1963, Dr. Scholtz joined the faculty at USC, where he is now Professor of Electrical Engineering. From 1984 to 1989, he served as Director of USC's Communication Sciences Institute. In 1996, he founded the Ultra-wide-Band Radio Laboratory as part of the Integrated Media Systems Center at USC. Currently, he is Chairman of the Electrical Engineering-Systems Department at USC. He has consulted for the LinCom Corporation, Axiomatix, Inc., the Jet Propulsion Laboratory, Technology Group, TRW, Pulson Communications, and Qualcomm, as well as various government agencies. He has co-authored *Spread Spectrum Communications* (Rockville, MD: Computer Science Press, 1985), with M. K. Simon, J. K. Omura, and B. K. Levitt, and *Basic Concepts in Information Theory and Coding* (New York: Plenum, 1984), with S. W. Golomb and R. E. Peile. His research interests include communication theory, synchronization, signal design, coding, adaptive processing, and pseudonoise generation, and their application to communications and radar systems.

In 1980, Dr. Scholtz was elected to the grade of Fellow in the IEEE "for contributions to the theory and design of synchronizable codes for communications and radar systems." He has been an active member of the IEEE for many years, manning important organizational posts, including Finance Chairman for the 1977 National Telecommunications Conference, Program Chairman for the 1981 International Symposium on Information Theory, and Board of Governors positions for the Information Theory Group and the Communications Society. In 1983, he received the Leonard G. Abraham Prize Paper Award for the historical article, "The Origins of Spread Spectrum Communications;" this same paper received the IEEE 1984 Donald G. Fink Prize Award. His paper "Acquisition of Spread-Spectrum Signals by an Adaptive Array" with D. M. Dlugos received the 1992 Senior Award from the IEEE Signal Processing Society. His paper "Strategies for minimizing the intercept time in a mobile communication network with directive/adaptive antennas," with J.-H. Oh received the Ellersick Award for the best unclassified paper at Milcom'97. His paper "ATM-Based Ultra-Wide Bandwidth (UWB) Multiple-Access Radio Network for Multimedia PCS" with students M. Z. Win, J. H. Ju, X. Qiu, and colleague V. O. K. Li received the Best Student Paper Award from the NetWorld+Interop'97 Program Committee.